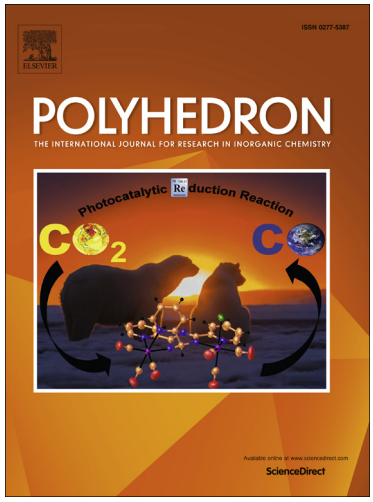

A new inorganic-organic nanohybrid based on a copper(II) semicarbazone complex and $PMo_{12}O_{40}^{3-}$ polyanion: synthesis, characterization, crystal structure and photocatalytic activity for degradation of cationic dyes

Saeed Farhadi, Farzaneh Mahmoudi, Michal Dusek, Vaclav Eigner, Monika Kucerakova

PII: S0277-5387(16)30625-8
DOI: http://dx.doi.org/10.1016/j.poly.2016.11.034
Reference: POLY 12342

To appear in: *Polyhedron*

Received Date: 2 September 2016
Revised Date: 18 November 2016
Accepted Date: 22 November 2016

Please cite this article as: S. Farhadi, F. Mahmoudi, M. Dusek, V. Eigner, M. Kucerakova, A new inorganic-organic nanohybrid based on a copper(II) semicarbazone complex and $PMo_{12}O_{40}^{3-}$ polyanion: synthesis, characterization, crystal structure and photocatalytic activity for degradation of cationic dyes, *Polyhedron* (2016), doi: http://dx.doi.org/10.1016/j.poly.2016.11.034

A new inorganic-organic nanohybrid based on a copper(II) semicarbazone complex and $PMo_{12}O_{40}^{3-}$ polyanion: synthesis, characterization, crystal structure and photocatalytic activity for degradation of cationic dyes

Saeed Farhadi[a]*, Farzaneh Mahmoudi[a], Michal Dusek[b], Vaclav Eigner[b], Monika Kucerakova[b]

[a] Department of Chemistry, Lorestan University, Khoramabad 68151-44316, Iran

[b] Institute of Physics of the Czech Academy of Sciences, Na Slovance 2, 18221 Prague 8, Czech Republic

*Corresponding author: Tel: +98 06633120611, fax: +98 06633120618.

Email address: sfarhadi1348@yahoo.com (S. Farhadi)

ABSTRACT

A new inorganic-organic nanohybrid based on Keggin-type polyoxomolybdate and a copper(II) semicarbazone complex, namely $[Cu_2(HL)_2(PMo_{12}O_{40})(OCH_3)_2(Cl)(H_2O)].8CH_3OH{\cdot}4H_2O$ [HL=pyridine-2-carbaldehyde semicarbazone] (**1**) was synthesized by a sonochemical method. The single crystal of (**1**) was synthesized with the branched tube method. The nanohybrid (**1**) was characterized by using FT-IR, PXRD, FESEM, TEM, EDX, UV-Vis, TG-DTA analysis and single-crystal X-ray diffraction. Single-crystal X-ray diffraction reveals that the $PMo_{12}O_{40}^{3-}$ cluster acts as a bidentate inorganic ligand and coordinates two symmetrically equivalent $[Cu(Cl)_{0.5}(HL)(OCH_3)(H_2O)_{0.5}]$ complexes. SEM and TEM images confirmed highly porous plate like morphology of the nanohybrid sample. To the best of our knowledge, the sample (**1**) represents the first example of a hybrid based on POMs and semicarbazone Schiff base complexes. The photocatalytic properties of nanohybrid (**1**) were investigated in detail and the results of photocatalytic experiments show it can be used as an efficient and recoverable photocatalyst for the complete degradation of cationic dyes as methylene blue (MB) and rhodamin B (RhB).

Keywords: Inorganic-organic hybrid, Semicarbazone complex, Nanohybrid, photodegradation, cationic dyes.

1. Introduction

Polyoxometalates (POMs) are typical class of metal-oxygen clusters, with an unmatched range of physical and chemical properties such as thermal and oxidative stability, Bronsted acidity and magnetic properties [1-6].The study of POMs is not only

interesting in terms of the molecular structural diversity but also regarding the wide range of applications in, e.g., separations, catalysis, magnetism, medicine, materials science, electrochemistry and macromolecular crystallography [7-15]. In this context, POMs with early transition metal-oxygen clusters have been attracting much attention [16-20]. The progress of POMs chemistry has been always closely associated with the functionalized POMs. The attachment of functional organic groups to POMs skeletons can improve properties of the resulting hybrid compounds [21-23]. The reported works indicate that the sizes, dimensions and other properties of these hybrid compounds are adjustable and can be controlled. Furthermore, synthesis of these hybrid compounds can also conquer the inherent drawbacks of bare POMs (such as low specific surface area and instability under the reaction conditions) [24-26]. To date, a series of hybrids constructed from POMs and various transition metal complexes, have indicated that the type of POMs, organic ligands, and transition metal ions all play important roles in the self-assembly processes [27-32]. In this regard, compared with other types of POMs, the classical Keggin polyanions $XM_{12}O_{40}^{n-}$ (X = B, P, Si and etc.; M = Mo or W) are one of the most important components. Selecting of organic ligand is crucial in the process of assembling inorganic-organic hybrid compounds, because the coordination atoms and the ligand geometry have influence on the final structures. To date N/O-donor ligands with strong coordination capacity have been used for the construction of POMs based hybrid compounds [33-41].

The semicarbazone Schiff base ligands can coordinate in the neutral or anionic forms and give rise to interesting hybrid compounds [42-44]. To our knowledge, there is still considerable gap in investigation of POMs-based inorganic-organic hybrid materials with these ligands. Studies have shown that POMs based inorganic-organic hybrid compounds

could be used as one kind of green and cheap photocatalysts for the removal of organic pollutants from water [45-50]. However, the design and synthesis of water-insoluble POMs-based hybrid photocatalysts is an intriguing project, due to oxygen-rich surfaces, high negative charges, the ease of their structure/property tuning, recovering and recycling, as well as efficient light energy utilization [51-61].

In this work, we have synthesized a new nanohybrid compound based on Cu(II)-pyridine-2-carbaldehyde semicarbazone complex, phosphomolybdic acid ($H_3PMo_{12}O_{40}$), formulated as $[Cu_2(HL)_2(PMo_{12}O_{40})(OCH_3)_2(Cl)(H_2O)].8CH_3OH{\cdot}4H_2O$ (**1**). In compound (**1**), the Cu(II)-HL complex is covalently bonded to Keggin-type $PMo_{12}O_{40}^{3-}$ polyanion. The nanohybrid powder of (**1**) was also synthesized by a sonochemical method and it was fully characterized by different techniques. In addition, the photocatalytic property of the nanohybrid (**1**) was evaluated for the degradation of organic dyes pollutants.

2. 1. Syntheses

Schiff base ligand HL [HL: $C_5H_5NCH{=}NNHCONH_2$] was prepared by condensation of pyridine-2-carbaldehyde with semicarbazide hydrochloride by the reflux method according to a literature procedure [42, 44]. Anal. Calc. for $C_7H_8N_4O$: C, 45.7; H, 4.5; N, 30.1%. Found: C, 45.9; H, 4.3; N, 30.3% .FT IR data (KBr, cm^{-1}): 3321 m, 3178 m, 1701 s, 1612 s, 1168 s,601 m, 455 m.

The nanohybrid (**1**) was synthesized by a sonochemical route as follows [62,63]: Accordingly, 10 mL methanolic solution of copper(II) acetate monohydrate (0.02 M) was sonicated in a high-density ultrasonic probe, operating at 20 kHz with a maximum power output of 200W. To this solution, 10 mL methanolic solution of HL (0.02 M) and 10 mL

methanolic solution of phosphomolybdic acid (0.001M) were added. The reaction mixture was sonicated for 30 min, then the produced green precipitate was collected, filtered and washed with methanol and air dried. Yield: 0.20 g, 70%. FT IR data (KBr, cm^{-1}): 3334 m, 1668 s, 1514 s, 1174 s,1062 s, 962 s, 877 s, 796 s, 597 m, 507 m.

In order to X-ray crystallographic study, the single crystal of (**1**) was prepared by a branched tube method [64,65]. Briefly, HL ligand (0.04 g, 0.2 mmol), copper (II) acetate monohydrate (0.04 g, 0.2 mmol) and phosphomolybdic acid (0.2 g, 0.1 mmol) dissolved in methanol (30 mL) were placed in the sealed branched tube and held in an oil bath at temperature of 60 °C, while the branch is at room temperature. After a week, green crystalline materials suitable for X-ray studies deposited in the branch were collected by filtration, washed with methanol and dried in air. Yield: 0.12 g, 43%. FT IR data (KBr, cm^{-1}): 3344 m, 1666 s, 1514 s, 1172 s,1062 s, 968 s, 877 s, 794 s, 597 m, 507 m.

2. 2. Characterization

Fourier-transform infrared spectra were recorded on Shimadzu FT-IR 8400S (Japan) with temperature controlled high sensitivity detector (DLATGS detector) and resolution of 4 cm^{-1} in the scan range of 500-4000 cm^{-1} using KBr pellet. The XRD patterns were obtained on a Rigaku D -max C III diffractometer using Ni-filtered Cu Kα radiation (λ =1.5406Å) for determination of the phases presents in the decomposed samples. UV-Vis spectra were recorded on a Carry 100 Varian spectrophotometer. SEM images were obtained from MIRA3 TESCAN Field Emission Scanning Electron Microscope equipped with a link Energy-Dispersive X-ray (EDX) analyzer. Vibrating sample magnetometer (VSM, Meghnatis Daghigh Kavir Company, Iran) was employed to measure the

magnetic parameter at room temperature. An ultrasonic generator (Bandeline GM 2200) equipped with a converter/transducer and titanium oscillator operating at 20 kHz with a maximum power output of 200 W was used for the ultrasonic irradiation. TEM images were recorded on a Philips CM120 microscope with LaB6 cathode operated at 120 kV, equipped with a CCD camera SIS Veleta. The Sample was placed on carbon-coated Cu grid.

2. 3. X-ray crystallographic study

Single-crystal X-ray diffraction data for compound **1** were recorded using kappa four-circle diffractometer Gemini of Oxford Diffraction equipped with a classical sealed X-ray tube with Mo anode, Mo-Enhance collimator and CCD detector Atlas S1. Data reduction was done with Crysalis [66] using the correction based on crystal shape followed by the correction based on spherical harmonic functions (ABSPACK). The structure was solved with Superflip [67] and refined with Jana 2006 [68].

As often observed for this kind of structures, symmetry-induced disorder of the $PMo_{12}O_{40}^{3-}$ polyanion cluster was present, described as the inversion of the cage through the inversion centre located at phosphorus. Disordered oxygen atoms had occupancy 0.5 forced by the symmetry. Other kind of disorder was found for one of the four molecules of methanol which had two possible orientations. In this case, the disorder was not induced by symmetry but occupancy of the two methanol molecules was approximately 1:1. We also found a region of disordered atoms O1w, O2w and O3w, where we speculated that this is lattice water. For these three atoms we refined a common U_{iso} parameter and three independent occupancy parameters, leading to approximately 4 molecules of water for Z=1. We fixed occupancy of the fully occupied O1w and restrained the sum of occupancy

parameters for O2w and O3w to keep 4 molecules exactly. However, it should be noted that modelling these molecules was unreliable but needed to obtain reliable difference Fourier maps. Finally, a mixed site was discovered among at the equatorial positions of the Cu1 coordination polyhedron. At the position not belonging to the tridentate ligand we originally expected coordinated water but scattering power of oxygen was as strong as magnesium. This situation was described as 1:1 mixed site of oxygen and chlorine because during the synthesis semicarbazide hydrochloride was used.

The non-hydrogen atoms were refined with harmonic displacement parameters (ellipsoids) except atoms of disordered methanol and disordered lattice water. Hydrogen atoms attached to carbon were kept at expected positions. Hydrogen atoms attached to N3l and N4l were found from the difference Fourier map. Refinement of the hydrogen atom on N3l was possible using only the usual N-H bond length restraint 0.86 Å, while for NH_2 (atom N4l) also the H-N-H angle had to be restrained to 120°. We could not determine hydrogen atoms attached to oxygen of methanol (O6, O10, O12, O29 /O42), hydrogen atoms of lattice water (O1w, O2w, O3w) and hydrogen atoms of the partially occupied coordinated water (O1). For these atoms no indication was found at the difference Fourier map and they were omitted from the structure model. The difference Fourier map was also plain at the section calculated through O8, Mo5 and O8 (1-x, -y, 1-x). These two oxygen atoms are as close as 2.8622(1) Å and we hoped to find hydrogen atom keeping them together. Unfortunately, this was not possible at the proximity of a cage composed of heavy atoms. The final refinement was oscillating. In order to reach the convergence, we had to use Marquart refinement method with the fudge factor 0.002 and with damping

151 factor 0.5. Refinement of 601 parameters using 8 restraints and 12357 independent
152 reflections resulted in final *R* factors $R_{(obs)}$ 0.035 and $wR_{(all)}$ 0.097.
153
154 **2. 4. Photocatalytic tests**
155 Photocatalytic ativity of the compound (**1**) was tested by choosing the
156 photodegradation of methylene blue (MB), Rhodamin B (RhB) and methyl orange (MO) dyes
157 in aqueous solutions under UV-visible light irradiation. The irradiation source was a 400W
158 high-pressure mercury lamp equipped with a cool water circulating filter to absorb the near
159 IR and a UV light cut-off filter in order to avoid direct photolysis of organic dyes ($\lambda \geq 420$
160 nm). The photocatalytic experiments were carried out in a cylindrical reactor of 100 mL
161 capacity, located at 15 cm distance from the lamp. For each experiment, reaction
162 suspensions were freshly prepared by adding 25 mg of the nanohybrid (**1**) and 2 mL of
163 H_2O_2 (0.1 mol/L) to 50 ml of aqueous dye solution with an initial concentration of 25
164 mg/L. Prior to photoreaction, the suspension was magnetically stirred in dark for 30 min to
165 attain adsorption/desorption equilibrium. The aqueous suspension containing dye and
166 photocatalyst was then irradiated by visible light with constant stirring. In 30 min intervals,
167 samples (2 mL) were taken from the reactor and centrifuged to remove the nanohybrid (**1**).
168 The concentration of MB, RhB and MO in the solution was determined by measuring the
169 absorbance at 664 nm for MB, 553 nm for RhB and 463 nm for MO as a function of
170 irradiation time by UV-vis spectroscopy. The degradation efficiency of dyes was
171 calculated according to the equation: $\eta\ (\%) = (A_0 - A_t)/A_0 \times 100$, where η is the
172 photocatalytic efficiency, A_0 is the absorbance intensity of the dye solution after the

adsorption-desorption equilibrium, and A_t is the absorbance intensity of dye after photocatalytic degradation in specified exposure time (t).

The control experiments in the presence of H_2O_2 alone (without (**1**) and in dark), H_2O_2/h*ν* (without (**1**)), (**1**)/h*ν* (without H_2O_2) and $H_2O_2/PMo_{12}O_{40}^{3-}$/h*ν* systems were done under similar conditions outlined above for MB dye degradation. The obtained results were compared with the H_2O_2/(**1**)/h*ν* system.

The recyclability of the nanohybrid (**1**) was studied under similar experiments described above at constant dye concentrations (50 ml, 25 mg/L) containing H_2O_2 (2 mL, 0.1 mol /L) and the recovered photocatalyst (20-25 mg) in each cycle. After the photocatalytic degradation experiments, the nanohybrid (**1**) photocatalyst was separated by simple centrifugation for its insoluble property in common solvents, washed with water and ethanol several times and dried at 80°C for overnight. Then, the recovered photocatalyst was reused in the next cycle.

3. Results and discussion

3.1. Structure description of compound (1)

X-ray single-crystal structural analysis revealed that the compound (**1**) with chemical formula of $[Cu_2(HL)_2(PMo_{12}O_{40})(OCH_3)_2(Cl)(H_2O)]\cdot 8CH_3OH\cdot 4H_2O$ crystallizes in the triclinic system with space group P-1. The refinement details are summarized in the Table 1. As observed in Fig .1, the structure of (**1**) contains one Keggin-type $PMo_{12}O_{40}^{3-}$ polyanion, two motifs of $[Cu(Cl)_{0.5}(HL)(OCH_3)(H_2O)_{0.5}]$ complex, eight free methanol molecules and four water molecules per unit cell. The $PMo_{12}O_{40}^{3-}$ is covalently bonded to

two $[Cu(Cl)_{0.5}(HL)(OCH_3)(H_2O)_{0.5}$ complex. The HL is in a neutral form and coordinated to Cu(II) center as a NNO donor tridentate ligand. The Cu1 center exhibits a distorted octahedral environment with equatorial sites occupied by two nitrogen and one oxygen atoms of the HL (N1l, N2l and O2l) and one oxygen atom of water molecule (O1l) or one chloride anion (Cl1l). The axial sites are occupied by one oxygen of methanol (O1s) and one oxygen atom of polyoxometalate (O2). Thus the coordination octahedron around Cu1l is axially elongated. The Cu(II)-N distances for the azomethine nitrogen atoms (Cu1l–N2l) are shorter than for the pyridyl nitrogen atoms (Cu1l–N1l) which indicates their stronger coordination to the metal ion. The Cu–O bond length connecting the complex with the polyoxometalate (Cu1l–O2) is longer in contrast with the Cu–O bond lengths within the complex (Cu1l–O1l, Cu1l–O2l) and to methanol (Cu1l–O1s). The $PMo_{12}O_{40}^{3-}$cluster acts as a bidentate inorganic ligand and coordinates two symmetrically equivalent $[Cu(Cl)_{0.5}(HL)(OCH_3)(H_2O)_{0.5}]$ complexes through the Cu–O–Mo bridge (Cu-O-Mo 135.61°, Cu–O2.692Å, and O1l–Mo2 1.661 Å). Furthermore, the $PMo_{12}O_{40}^{3-}$ units are coordinated to four adjacent $[PMo_{12}O_{40}]^{3-}$, with its four noncoordinated terminal oxygen atoms by short contacts, with bond distance in range of 2.864-2.899 Å forming a layers in the structure.

Fig. 1.

The $PMo_{12}O_{40}^{3-}$ polyanion is a well-known α-Keggin structure composed of twelve corner sharing MoO_6 octahedral with the central phosphorus atom coordinated to four oxygen atoms in a distorted tetrahedral fashion. The Mo–O distances can be classified as follows: Mo–O_t (terminal oxygen) of , Mo–O_b (bridging oxygen) of , Mo–O_c (central oxygen). The distances found in the structure are consistent with those described in the

literature. For the further information on the geometry of the polyoxometalate see Table S1. There are several hydrogen bonds in structure. However their full characterization cannot be done due to the absence of hydrogen atoms of solvent molecules. The most important intermolecular hydrogen bonds are between terminal oxygen atoms of $PMo_{12}O_{40}^{3-}$ units with free methanol molecules which expand the structure of **1**, in three dimensions (Fig. 2.). For more details on hydrogen bonding see Table 2.

Fig. 2.

Table 1 and Table 2

3.2. FT-IR and XRD analyses

The FT-IR spectra of free HL, PMo_{12} polyanion and compound (**1**) (in both forms: single crystal and nanohybrid powder) are shown in Fig. 3. Bands in the region of 1100 to 1608 cm^{-1} can be ascribed to the characteristic peaks of HL ligand (Fig. 3(a)) [42,44]. The strong bands of PMo_{12} is assigned at 780-1070 cm^{-1} (Fig. 3(b)). As shown in Fig. 3(c) and (d), both forms of compound (**1**) show the characteristic bands of HL and $PMo_{12}O_{40}^{3-}$ polyanion. The $P–O_a$ vibrations are observed at 1062 cm^{-1}. Furthermore, the strong band at 794, 877, 968 cm^{-1} for single crystal (**1**) and also the observed peaks at 796, 877, 962 cm^{-1} for nanohybrid (**1**), are attributed to $Mo–O_b–Mo$, $Mo–O_a–Mo$ and $Mo=O_t$ bond stretching vibrations of PMo_{12} polyanion, respectively.

Fig. 3.

The experimental and simulated XRD patterns of (**1**) are presented in Fig. 4(a)-(c). Their peak positions are in good agreement with each other, reveals the phase purity and similarity of the samples. The partial differences in relative intensities may be due to the

preferred orientation in the powder sample. The average size of the particles were estimated to be 30-50 nm using the Scherrer formula $D=0.891\lambda/\beta\cos\theta$, where D is the average grain size, λ the X-ray wavelength (1.5418 Å), β the full-width at half maximum of an observed peak and θ its diffraction angle.

[Fig. 4.]

3. 3. Morphology of nanohybrid (1)

The shape and morphology of the hybrid (**1**) were investigated in details by using SEM and TEM, as shown in Fig. 6. From the SEM images in Fig. 5(a) and (b), it is clearly evident that the product consists of extremely fine nanostructures with plate-like morphologies that appreciably aggregated as clusters due to the extremely small dimensions and high surface energy of the obtained nanoparticles. We also can find from this figure that the morphology of the particles is almost homogeneous. The SEM images confirm that these plates undergo further aggregation to form porous agglomerate structure. Fig. 5(c) shows TEM images of (**1**) in different scales. The TEM sample was prepared by dispersing the nanohybrid powder in ethanol by ultrasonic vibration. It can be seen from Fig. 5(c) that the product shows approximately plate-like morphologies with a uniform size. The TEM images show that the product was formed mainly from nanoplates with lengths of 200-600 nm and thicknesses of 40–50 nm.

[Fig. 5]

Additionally, the chemical purity and stoichiometry of the (**1**) were verified by EDX analysis. The EDX spectra in Fig. 6(a) and (b) confirm the existence of Cu, C, N, O, P and Mo elements in the structure of single crystal and nanohybrid of (**1**), respectively. As seen in the insets, the single crystal and nanohybrid (**1**) show very similar

atomic percentages, confirming that they have the same composition without any impurity. Furthermore, the elemental mapping images of and single crystal and nanohybrid (**1**) in Fig. S1 and Fig. S2 show that Cu, C, N, O, P, and Mo elements are uniformly distributed in throughout of the samples.

3. 4. Thermal analysis

The thermal analysis (TG-DTA) of the single crystal and nanohybrid **1** was performed in static air atmosphere with a heating rate of 10 °C/min at the temperature of 40-900 °C (Fig. 7). The TG-DTA curves of single crystal (**1**) exhibits three weight loss steps as shown in Fig. 7(a). The first weight loss of 7% (calc. 7.3%) below 200 °C corresponds to the loss of non-coordinated methanol molecules. The second and third weight loss of 16.5 % (calc. 17%) occurred in the range of 220–470 °C in TG curve with an exothermic peak in the DTA curve, are attributed to the decomposition of HL ligands and the coordinated methanol molecules. Collapse of PMo_{12} clusters occurs in the range of 470–760 °C without any weight loss in TG curve. For the Collapse of PMo_{12} clusters, an endothermic peak is observed in the DTA curve. These results are in good agreement with the structural formula of compound **1** obtained from single crystal X-ray diffraction. As observed in Fig. 7(b), the TG-DTA curves of the nanohybrid (**1**) show very similar behavior with those of the single crystal. However, the nanohybrid (**1**) is less stable and their decomposition steps are shifted about 7-10 °C toward lower temperatures, which is in agreement with previous reports [69,70].

[Fig. 7]

3. 5. Optical absorption properties

The UV-Vis spectra of HL, $PMo_{12}O_{40}^{3-}$ and nanohybrid (**1**) were measured in the range of 200 to 500 nm as shown in Fig. 8. In UV-Vis spectrum of HL (Fig. 8(a)), the observed bands at 210 and 300 nm are attributed to $\pi \rightarrow \pi^*_{pyridine}$ and $\pi \rightarrow \pi^*_{imine}$ of HL. As can be seen in Fig. 8(b), the pure $PMo_{12}O_{40}^{3-}$ demonstrates a sharp absorption band at 220-240 nm and a broad band at 270-380 nm corresponds to $O_{b/c} \rightarrow$Mo charge transfer. In the spectrum of nanohybrid (**1**), all the characteristic bands of HL and PMo_{12} are observed with a red shift, confirming the presence of strong chemical interactions between the polyanion and Cu(II)-HL complex (Fig. 8(a)). As can be observed, linking the complex to $PMo_{12}O_{40}^{3-}$ resulted in the enhancement of optical absorption in the region of 300–440 nm. This is the reason for the high photocatalytic activity of (**1**) compared with the pure $PMo_{12}O_{40}^{3-}$.

[Fig. 8]

3. 6. Photocatalytic activity

The photocatalytic activity is an attractive property of hybrid compounds based on POMs for the removal of organic pollutants from water [14, 15, 35]. To evaluate the photocatalytic ability of (**1**) for the degradation of dyes from contaminated water, MB, RhB and MO with different charges and sizes as the typical organic pollutant targets were selected for experiments. The degradation experiments were carried out, in presence of H_2O_2 as an efficient and green oxidant. Fig. 9 shows the changes in the absorption spectra of dyes as a function of irradiation time. In the presence of (**1**) as a photcatalyst and H_2O_2, the MB was reduced, and the intensity of the absorption peak at 664 nm decreased gradually with time and after about 240 min it almost disappeared (Fig. 9(a)). The intense blue colour of the initial solution disappears and becomes almost colourless, indicating the photo-degradation process of MB. Furthermore, the absorption band of MB at 664 nm

were not shifted during the degradation process, indicating the degradation of MB is due to chronophers being destroyed [63,64]. Similar behavior was observed for the RhB dye. It is obvious that the absorption peak of RhB at 554 nm decreased significantly as time increases, indicating the efficient degradation of this cationic dye in the presence of the nanohybrid (**1**). The nanohybrid (**1**) was also tested for the photocatalytic degradation of anionic MO dye with a characteristic absorption peak at 463 nm. As can be seen in Fig. 9(c), the colour of MO solution changed immediately from orange to red and then it remains unchanged during irradiation in presence of (**1**) for 240 min. At the same time, the adsorption peak of MO was shifted to 502 nm. This red shift can be attributed to the decrease of pH value probably due to the existence of polyanion units in the hybrid network. Furthermore, the degradation rates (C/C_0) of dyes as a function of irradiation time are compared in Fig. 9(d). After irradiation for 240 min, the photocatalytic degradation rates, are 96% for MB, 84 % for RhB, 18% for MO, respectively. Furthermore, the degradation rate curves for MB and RhB are nearly linear. The obtanedresults confirm that nanohybrid (**1**) is an effective photocatalyst for the degradation of cationic organic dyes. The slow degradation efficiency of MO can be related to its high redox potential, hence this system is not efficient photcatalyst for degradation of anionic MO dye.

[Fig. 9]

Accordingly, a series of control experiments were conducted. From Fig. 10, it is clear that the degradation percentages of MB in the presence of H_2O_2 alone (in dark), H_2O_2/hν, H_2O_2/(**1**)/hν, (**1**)/hν and $PMo_{12}O_{40}^{3-}$/hν systems were 7, 12, 96, 58, and 32 %, respectively, within 240 min of irradiation. As observed in Fig. 10,

among various used systems, almost complete degradation of MB was achieved in the presence of H_2O_2/(**1**)/hν system. On the other hand, the photocatalytic degradation percentage of MB decreased to 58% when H_2O_2 was omitted from this system. This result indicates that H_2O_2 is an efficient electron-acceptor in the heterogeneous (**1**) system. Meanwhile, the degradation efficiency in the presence of only H_2O_2/hν (without **1**) was very low (12 %), implying that (**1**) is an effective photocatalyst.

[Fig. 10.]

Based on the above experimental results and previously reported mechanisms [29, 35, 37], the possible mechanism of dyes photodegradation in the presence of (**1**) can be explained as follow: POMs exhibit semiconductor-like photochemical behaviors due to analogous electronic characteristics (band gap transition for semiconductors and HOMO–LUMO transition for POMs). Initially, the UV-visible light induce $PMo_{12}O_{40}^{3-}$ polyanion in nanohybrid (**1**) to produce oxygen-to-metal charge transfer (OMCT) with promoting electron from the highest occupied molecular orbital (HOMO) to the lowest unoccupied molecular orbital (LUMO) (Eq. (1)). The charge-transfer excited state ($[PMo_{12}O_{40}^{3-}]^*$) with strong oxidizing properties can direct oxidize the target dye pollutant, or react with other electron donors to accept the electrons and deposit them in its LUMO (Eq. (2)). The adsorbed H_2O_2 and O_2 molecules can easily trap an electron in LUMO of the reduced $PMo_{12}O_{40}^{4-}$ to yield the oxidizing species, $^{\bullet}OH$ and O_2^{-}, respectively (Eqs. (3) and (4)). Then, radicals attack organic substrates and degrade dye molecules (Eq. (5)).

$$PMo_{12}O_{40}^{3-} + h\upsilon \longrightarrow [PMo_{12}O_{40}^{3-}]^* \quad (1)$$

$$[PMo_{12}O_{40}^{3-}]^* + \text{dye} \longrightarrow PMo_{12}O_{40}^{4-} + \text{dye}^+ \quad (2)$$

$$PMo_{12}O_{40}^{4-} + H_2O_2 \longrightarrow PMo_{12}O_{40}^{3-} + OH^- + {}^{\bullet}OH \quad (3)$$

$$PMo_{12}O_{40}^{4-} + O_2 \longrightarrow PMo_{12}O_{40}^{3-} + {}^{\bullet}O_2^- \quad (4)$$

dye /dye^{+} + $^{\bullet}OH/^{\bullet}O_2^{-}$ ⟶ degradation products (CO_2 + H_2O+ ...) (5)

3. 7. Reusability of the photocatalyst (1)

The reusability of catalysts is a very important parameter to assess the photocatalyst practicability. Unlike the bare $PMo_{12}O_{40}^{3-}$ which is soluble in water, the synthesized nanohybrid (**1**) is insoluble and can be separated from the reaction mixture by simple centrifugation. The reusability tests were carried out for the degradation of MB and RhB dyes for three cycles as presented in Fig. 11. It was observed that the degradation efficiency decreased from 97% to 96% for MB and from 86 to 83 for RhB after three cycles, which shows that the photocatalytic activity has a good repeatability and the considerable stability of the photocatalyst under the present conditions. The Kegging-type $PMo_{12}O_{40}^{3-}$ polyanions are covalently bonded to two Cu(II)-HL complexes and have extensive hydrogen bond interactions with other Cu(II)-HL complex molecules (see Figs. 1 and 2). Then, the $PMo_{12}O_{40}^{3-}$ units don't easily leak from the system. In a word, the photocatalyst not only has a good photocatalytic activity under UV-visible light, but also has good reproducibility of photocatalytic degradation by a simple recycled procedure, which are of great significance for practical use of the photocatalyst.

Fig. 11.

4. Conclusions

In conclusion, a new hybrid compound based on a copper(II)-semicarbazone Schiff base complex and a Keggin-type POM has been synthesized. This is the first report on the synthesis of hybrid compounds containing a POM and metal semicarbazone Schiff base complexes. The hydrogen bonds present in the structure have an important influence on linking the $PMo_{12}O_{40}^{3-}$ polyanions and coordination complex,

[$Cu(HL)(OCH_3)(Cl)_{0.5}(H_2O)_{0.5}$] to give a supramolecular network. The photocatalytic results confirmed that the nanohybrid (**1**) can degrade the cationic organic dyes with high efficiency. It was reused for at least three runs without significant loss of its catalytic activity. Furthermore, comparison studies revealed that the prepared nanohybrid had a higher photocatalytic activity than pure $PMo_{12}O_{40}^{3-}$. This study presents a green, low-cost, simple, procedure for the degradation of dye pollutants in aqueous wastewater solutions.

Acknowledgements

We thank the Lorestan University for the support of this work. The structure analysis was supported by the project 14-03276S of the Czech Science Foundation using instruments of the ASTRA lab established within the Operation program Prague Competitiveness project CZ.2.16/3.1.00/24510. Also, we are so thankful to Dr. Marketa Jarosova (Institute of Physics of the Czech Academy of Sciences) for valuable assistance.

Appendix A. Supplementary data

CCDC 1501912 contains the supplementary crystallographic data for the structure reported in this paper. These data can be obtained free of charge via http://www.ccdc.cam.ac.uk/conts/retrieving.html, or from the Cambridge Crystallographic Data Centre, 12 Union Road, Cambridge CB2 1EZ, UK; fax: (+44) 1223-336-033; or e-mail:deposit@ccdc.cam.ac.uk.

References

[1] H. Pang, Y. Niu, J. Yu, H. Ma, Q. Song, Sh. Li, Inorg. Chem. Commun. 59 (2015) 5–8.

[2] X.Wu, T. Huang, Zh. Xie, R. Zhao, Q. Wu, W. Yan, Mater. Lett. 154 (2015) 156–159.

[3] D.Y. Du, J.Sh. Qin, S.L. Li, Z.M. Su, Y.Q. Lan, Chem Soc Rev. 43 (2014) 4615–32.

[4] P. Putaj, F. Lefebvre, Coord. Chem. Rev. 255 (2011) 1642–1685.
[5] Y. Guo, Ch. Hu, J. Mol. Catal. A: Chem. 262 (2007) 136–148.
[6] X.Y. Yu, X. Cui, J. Lu, Y.H. Luo, H. Zhang, W.P. Gao, J. Solid State Chem. 209 (2014) 97–104.
[7] G. Hu, H. Miao, H. Mei, Sh. Zhou, Y. Xu, Dalton Trans. 45 (2016) 7947–7951.
[8] Z.J. Liu, Sh. Yao, Z.M. Zhang, E.B. Wang, RSC Adv. 3 (2013) 20829–20835.
[9] T.P. Hu,Y.Q. Zhao, K. Mei, S.J. Lin, X.P. Wang, D. Sun, Cryst. Eng. Commun. 17 (2015) 5947–5952.
[10] M. Ammam, J. Mater. Chem. A 1 (2013) 6291–6312.
[11] X.J. Dui, X.Y. Wu, J. Zh Liao, T. Teng, W.M Wu, W.B. Yang, Inorg. Chem. Commun. 56 (2015) 112–115.
[12] H. Dong, Y. Yang, F. Zhao, W. Ji, B. Liu, H. Hu, Y. Wang, H. Huang, Y. Liu, Zh. Kang, Inorg. Chem. Commun. 44 (2014) 107–110.
[13] R. Sivakumar, J. Thomas, M. Yoon, Journal of Photochemistry and Photobiology C: Photochemistry Reviews 13 (2012) 277– 298.
[14] W. Zhu, X.Y. Yang, Y.H. Yi, Inorg. Chem. Commun. 49 (2014) 159–162.
[15] Q. Zhai, L. Zhang, X. Zhao, H. Chen, D. Yin, J. Li, Appl. Surf. Sci. 377 (2016) 17–22.
[16] L. Zhang, B. Shan, H. Yang, D. Wu, R. Zhu, J. Nie, R. Cao, RSC Adv. 5 (2015) 23556-23562.
[17] F. Bamoharram, A. Ahmadpour, M.M. Heravi, A. Ayati, H. Rashidi, B. Tanhaei, Synth. React. Inog. Met.-Org. Chem. 42 (2012) 209–230.
[18] B.L. Fei, W. Li, J.H. Wang, Q.B. Liu, J.Y. Long, Y.G. Li, K.Z. Shao, Z.M. Su, W.Y. Sun, Dalton Trans. 43 (2014) 10005–10012.
[19] Y. Hua, G. Chen, X. Xu, X. Zou, J. Liu, B. Wang, Z. Zhao, Y. Chen, C. Wang, X. Liu, J. Phys. Chem. C 118 (2014) 8877–8884.
[20] L. Zhang, B. Shan, H. Yang, D. Wu, R. Zhu, J. Nie, R. Cao, RSC Adv. 5 (2015) 23556–23562.
[21] X. Wang, A. Tian, X. Wang, RSC Adv. 5 (2015) 41155–41168.
[22] S.S. Wang, G.Y. Yang, Chem. Rev. 115 (2015) 4893– 4962.
[23] G. Li, C. Salim, H. Hinode, Solid State Sci. 10 (2008) 121–128.
[24] H. Dong, Y. Yang, F. Zhao, W. Ji, B. Liu, H. Hu, Y. Wang, H. Huang, Y. Liu, Zh. Kang, Inorg. Chem. Commun. 44 (2014) 107–110.
[25] S.L. James, Chem. Soc. Rev. 32 (2003) 276-288.
[26] M.X. Yang, Sh. Lin, L.J. Chen, X.H. Chen, X.H. Yang, J. Guo, Polyhedron 87 (2015) 329–337.

[27] S.T. Zheng, J. Zhang, G.Y. Yang, Angew. Chem. Int. Ed. 47 (2008) 3909–3913.
[28] Y.Q. Jia, Ch. Qin, C.Y. Sun, K.Z. Shao, P.J. Liu, P. Huang, K. Zhou, Z.M. Su, Inorg. Chem. Commun. 20 (2012) 273–276.
[29] X.J. Dui, X.Y. Wu, T. Teng, L. Zhang, H.F. Chen, W.B. Yang, C.Z. Lu, Inorg. Chem. Commun. 55 (2015) 108–111.
[30] H. Pang, Y. Niu, J. Yu, H. Ma, Q. Song, Sh. Li, Inorg. Chem. Commun. 59 (2015) 5–8.
[31] W.Q. Kan, J.M. Xu, Y.H. Kan, J. Gao, S.Zh. Wen, J. Coord. Chem. 67 (2014) 195–214.
[32] T. Ito, Crystals 6, 24 (2016) 1–21.
[33] J. Tian, T. Jing,Y. Zheng, Z. Naturforsch 70 (2015) 461–466.
[34] H. Pang, Y. Niu, J. Yu, H. Ma, Q. Song, Sh. Li, Inorg. Chem. Commun. 59 (2015) 5–8.
[35] J.Q. Sha, B.B. Zhou, Ch. Wang, J.W. Sun, P.F. Yan, Solid state Sci. 40 (2015) 77–83.
[36] X.Y. Yu, X.B. Cui, J. Lu, Y.H. Luo, H. Zhang, W.P. Gao, J. Solid Statte Chem. 209 (2014) 97–104.
[37] D. Meziani, K. Abdmeziem, S. Bouacida, M. Trari, H. Merazig, Sol. Energy Mater. Sol. Cells 147 (2016) 46–52.
[38] F.Y. Yi, W. Zhu, S. Dang, J.P. Li, D. wu, Y.H. Li, Zh.M. Sun, Chem. Commun. 51 (2015) 3336–3339.
[39] M.T. Li, J.Q. Sha, X.M. Zong, J.W. Sun, P.F. Yan, L. Li, X.N. Yang, Cryst. Growth Des. 14 (2014) 2797–2802.
[40] Q. Lan, Y. Lu, Y.G. Li, H.Q. Tan, D. Liu, E.B. Wang, Trans. Met. Chem. 37 (2012) 445–451.
[41] Ch.G. Liu, T. Zheng, Sh. Liu, H.Y. Zhang, J. Mol. Struct. 1110 (2016) 44–52.
[42] S. Farhadi, F. Mahmoudi, J. Simpson, J. Mol. Struct. 1108 (2016) 583–589.
[43] B. Shaabani, A.A. Khandar, F. Mahmoudi, M.A. Maestro, S.S. Balula, L. Cunha-Silva, Polyhedron 57 (2013) 118–126
[44] B. Shaabani, A.A. Khandar, M. Dusek, M. Pojarova, F. Mahmoudi, A. Feher, M. Kajňaková, J. Coord. Chem. 66 (2013) 748–762.
[45] M. Mirzaei, H. Eshtiagh-Hosseini, M. Alipour, A. Frontera, Coord. Chem. Rev. 275 (2014) 1–18.
[46] V. Mirkhani, M. Moghadam, S. Tangestaninejad, I. Mohammad poor, N. Rasouli, Catal. Commun. 9 (2008) 219–223.
[47] Y. Bai, G.Q. Zhang, D.B. Dang, P.T. Ma, H. Gao, J.Y. Niu, Cryst. Eng. Commun. 13 (2011) 4181–4187.
[48] Q. Wu, W.L. Chen, D. Liu, C. Liang, Y.G. Li, S.W. Lin, E. Wang, Dalton Trans. 40 (2011) 56 – 61.

[49] S. Saha, P.P. Jana, C.J. Gómez-García, K. Harms, H. Pada Nayek, Polyhedron 104 (2016) 58–62.

[50] X. Meng, H.N. Wang, G.S. Yang, S. Wang, X.L. Wang, K.Z. Shao, Zh.M. Su, Inorg. Chem. Commun. 14 (2011) 1418–1421.

[51] S. Ou, J.P. Zheng, G.Q. Kong, Ch.D. Wu, Dalton Trans. 44 (2015) 7862–7869.

[52] A. Kar, Y.R. Smith, V. Subramanian, Environ. Sci. Technol. 43 (2009) 3260–3265.

[53] Z.J. Liu, Sh. Yao, Z.M. Zhang, E.B. Wang, RSC Adv. 3 (2013) 20829 –20835.

[54] C. Wang, Z. Xie, K.E. dekrafft, W. Lin, J. Am. Chem. Soc. 133 (2013) 13445–13454.

[55] X. Wang, Zh. Chang, H. Lin, A. Tian, G. Liu, J. Zhang, Dalton Trans. 43 (2014) 12272–12278.

[56] X. Wang, X. Liu, A. Tian, J. Ying, H. Lin, G. Liu, Q. Gao, Dalton Trans. 41 (2012) 3599 – 3615.

[57] Y.Q. Jiao, C. Qin, H.Y. Zang, W.Ch. Chen, Ch.G. Wang, T.T. Zheng, K.Z. Shao, Z.M. Su, Cryst. Eng. Commun. 17 (2015) 2176–2189.

[58] Sh. Li, L. Zhang, K.P. Ohalloran, H. Ma, H. Pang, Dalton Trans. 44 (2015) 2062–2065.

[59] X. Xu, X. Gao, T. Lu, X. Liu, X. Wang, J. Mater. Chem. A 3 (2015) 198–206.

[60] B. Liu, Z.Yu, J. Yang, W. Hu, Y.Liu, J. Ma, Inorg. Chem. 50 (2011) 8967–8972.

[61] S. Wan, K. Yu, L. Wang, Zh. Su, B. Zhou, Inorg. Chem. Commun. 61 (2015) 113–117.

[62] H. Sadeghzadeh, A. Morsali, V.T. Yilmaz, O. Buyukgungor, Ultrason. Sonochem. 17 (2010) 592–597.

[63] H. Sadeghzadeh, A. Morsali, V.T. Yilmaz, O. Buyukgungor, Inorg. Chim. Acta 363 (2010) 841–845.

[64] J.M. Harrowfield, H. Miyamae, B.W. Skelton, A.A. Soudi, A.H. White. Aust. J. Chem. 49 (1996) 1029–1042.

[65] F. Marandi, B. Mirtamizdoust, A.A. Soudi, H.K. Fun, Inorg. Chem. Commun. 10 (2007) 174–177.

[66] Rigaku Oxford Diffraction, Crys FAlis PRO. Rigaku Oxford Diffraction, Yarnton, England (2015).

[67] L. Palatinus, G. Chapuis, J. Appl. Cryst. 40 (2007) 786–790.

[68] V. Petricek, M. Dusek, L. Palatinus, Z. Kristallogr 229 (5) (2014) 345–352.

[69] A. Shahrjerdi, S.S. Hosseiny-Davarani, E. Najafi, M.M. Amini, Ultrason. Sonochem. 22 (2015) 382–390.

[70] S. Karimi-Behzad, E. Najafi, M.M. Amini, S. W. Ng, Monatsh. Chem. 146 (2015) 571–580.

Table 1. Crystal data and structure refinement parameters for **1**.

Chemical formula	C16 H24 Cl Cu2 Mo12 N8 O45 P, 2(O1.78), 8(CH3O)
Formula weight	2705.51
Crystal description	Block, green
Crystal size (mm)	0.17 x 0.17 x 0.09
Temperature (K)	120
Crystal system	Triclinic
Space group	P -1
a (Å)	10.8792(2)
b (Å)	12.7372(2)
c (Å)	13.9282(2)
α (°)	74.735(2)
β(°)	81.172(1)
γ(°)	73.495(2)
Volume (Å3)	1778.75(6)
Z	1
ρ calculated (g cm-3)	2.526
μ (mm-1)	2.798
Tmin,Tmax	0.620,0.778
Theta(max)	33.340
R(reflections)	0.0348(9849)
wR2(reflections)	0.0969(12357)

Table 2. List of selected hydrogen bonds (Å, °) in **1**.

D–H···A	D–H	H···A	D ···A	D–H···A
N3l–H1n3l···O14^{i}	0.86 (2)	2.01 (3)	2.708 (8)	137.1 (19)
N4l–H1n4l···O2s^{ii}	0.860 (8)	1.982 (9)	2.825 (4)	166.4 (9)
N4l–H2n4l···O2l^{iii}	0.860 (6)	2.069 (7)	2.917 (4)	168.7 (3)
C2l–H1c2l···O9'^{i}	0.96	2.37	3.137 (8)	137
C4l–H1c4l···O13^{iv}	0.96	2.50	3.429 (7)	164
C4l–H1c4l···O13^{iv}	0.96	2.40	3.312 (7)	159

Symmetry code: (*i*) -*x*+2, -*y*+1, -*z*+1; (*ii*) *x*+1, *y*, *z*; (*iii*) -*x*+2, -*y*+1, -*z*; (*iv*) -*x*+2, -*y*, -*z*+1

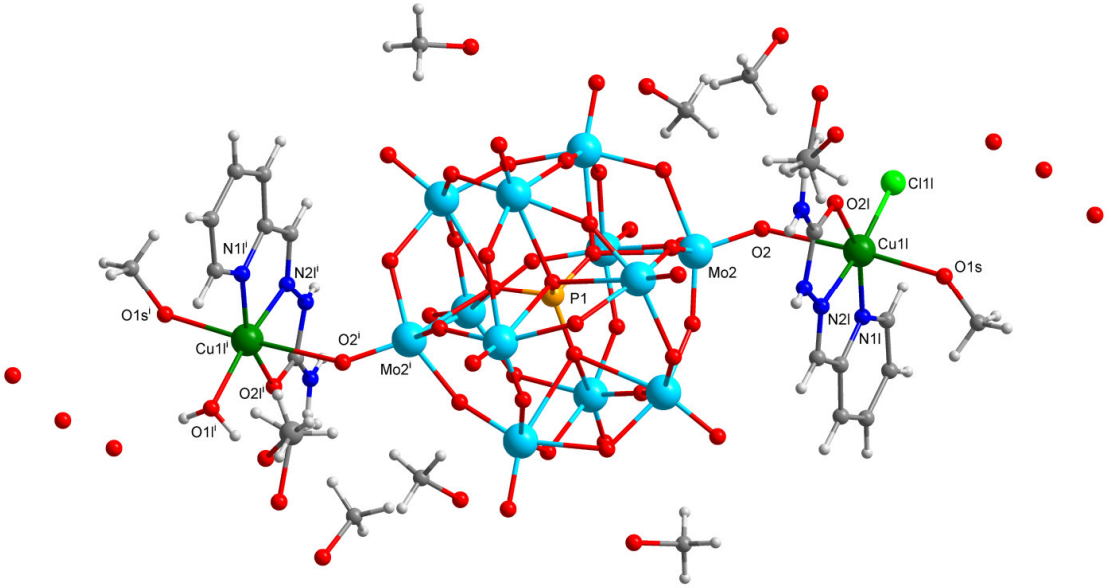

Fig. 1. View of the structure and the coordination environment of (**1**) (Symmetry code: (*i*) -*x*+1, -*y*+1, -*z*+1).

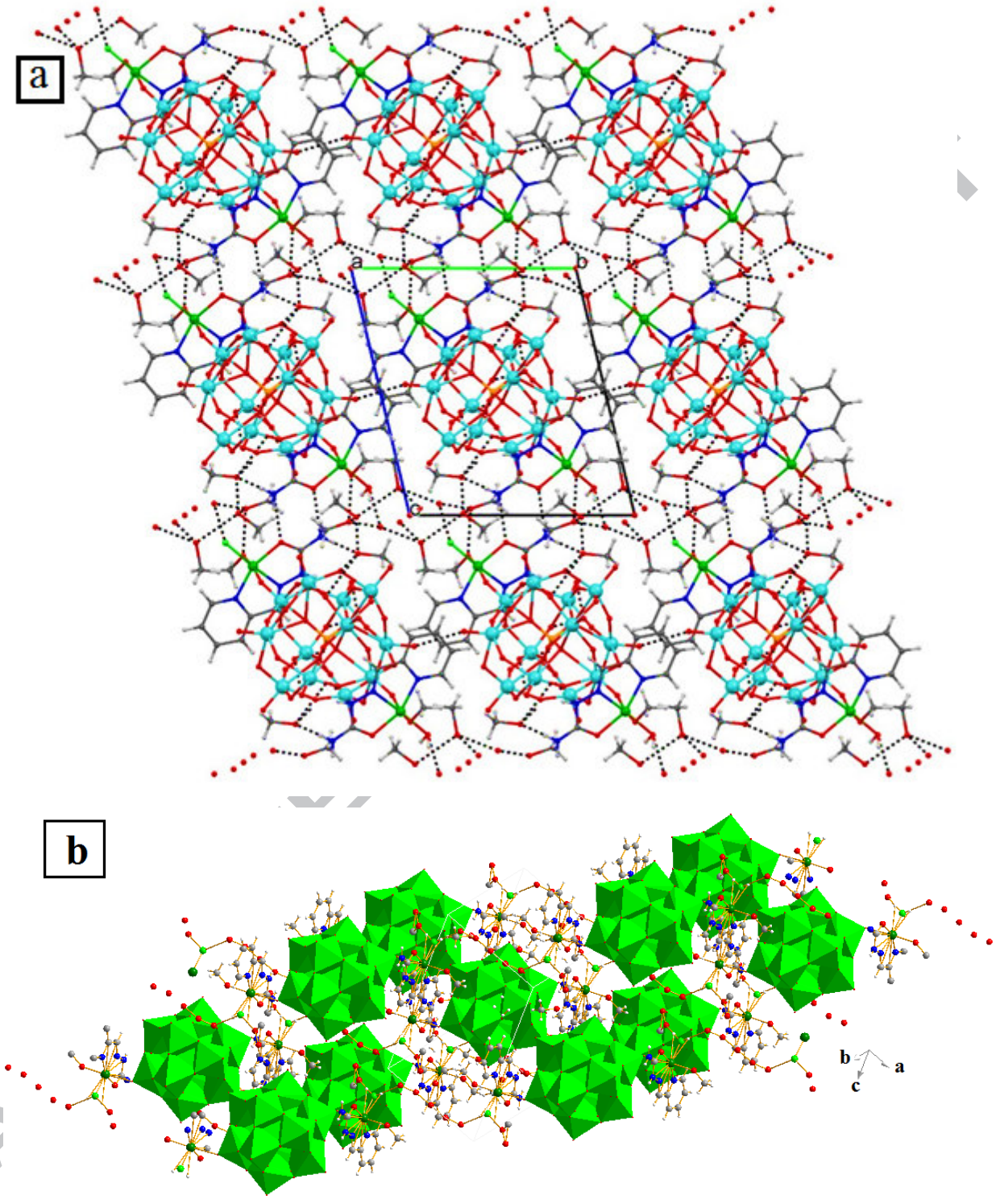

Fig. 2. (a) and (b) View of 3D supramolecular network of (**1**) expanded with the hydrogen bonding interactions.

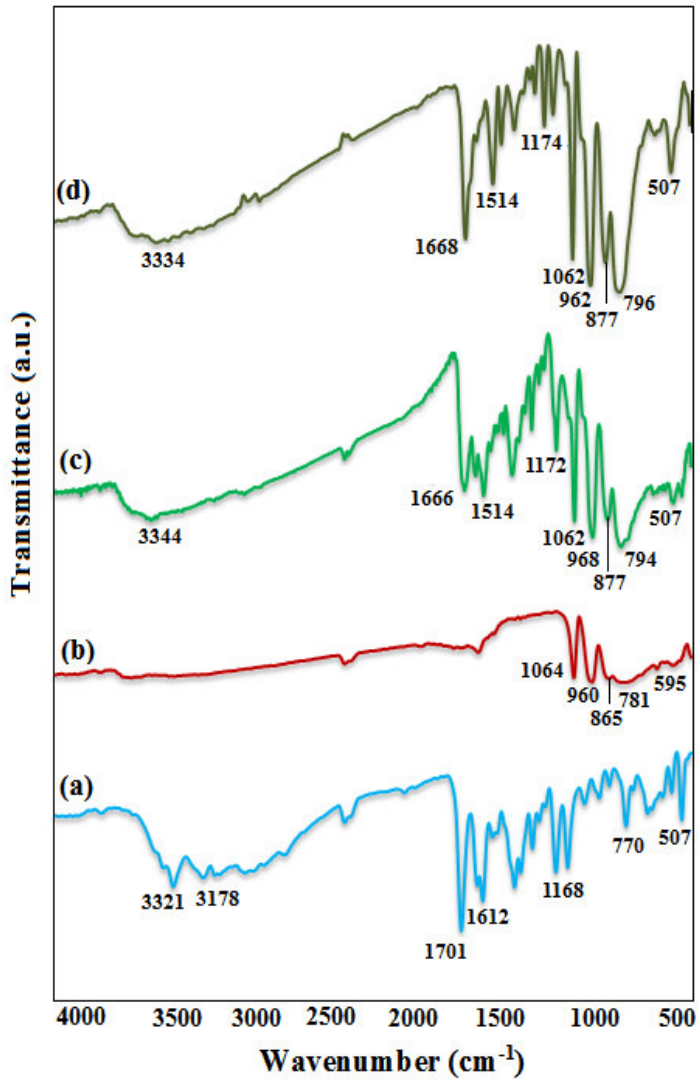

Fig. 3. The FT-IR spectra of: (a) HL ligand, (b) $PMo_{12}O_{40}^{3-}$ polyanion, (c) compound (**1**) in single crystal form and (d) compound (**1**) in nanohybrid powder form.

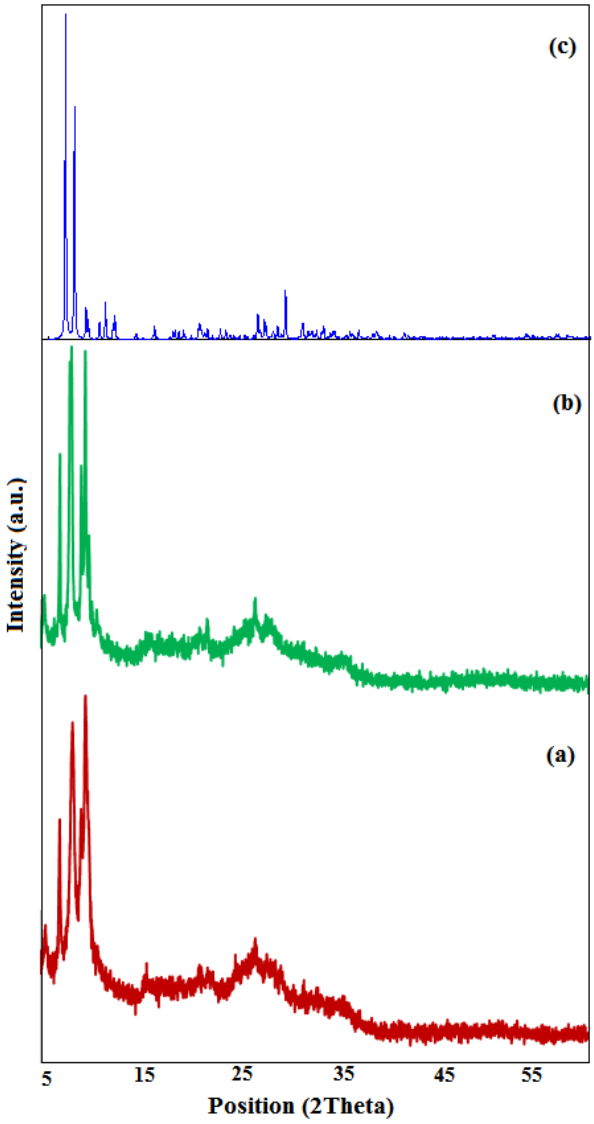

Fig. 4. PXRD patterns of (**1**)**:** (a) as nanohybrid powder, (b) as single crystal and (c) simulated pattern from single crystal X-ray data.

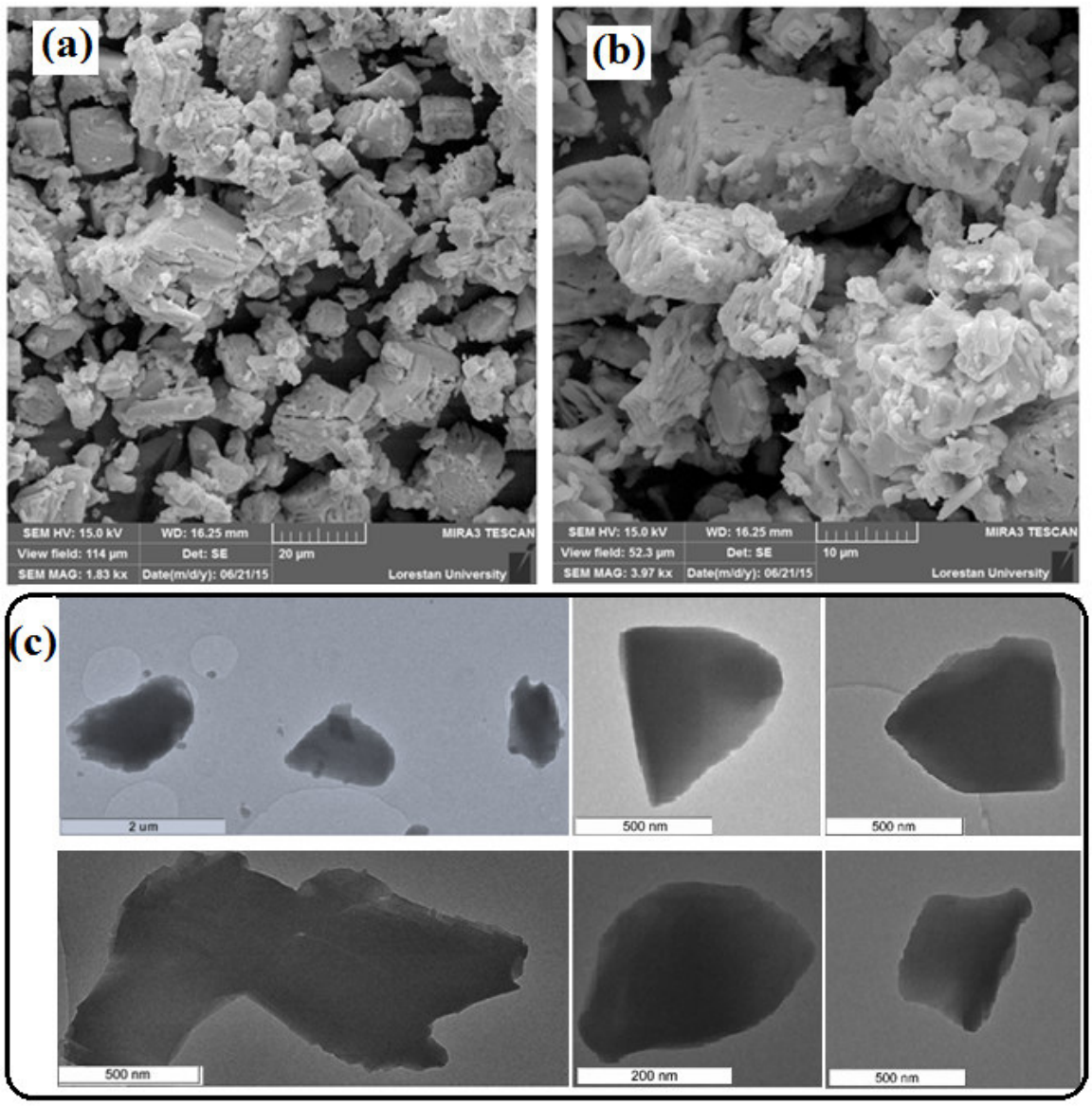

Fig. 5. (a) and (b) FESEM images and (c) TEM images of the nanohybrid (**1**).

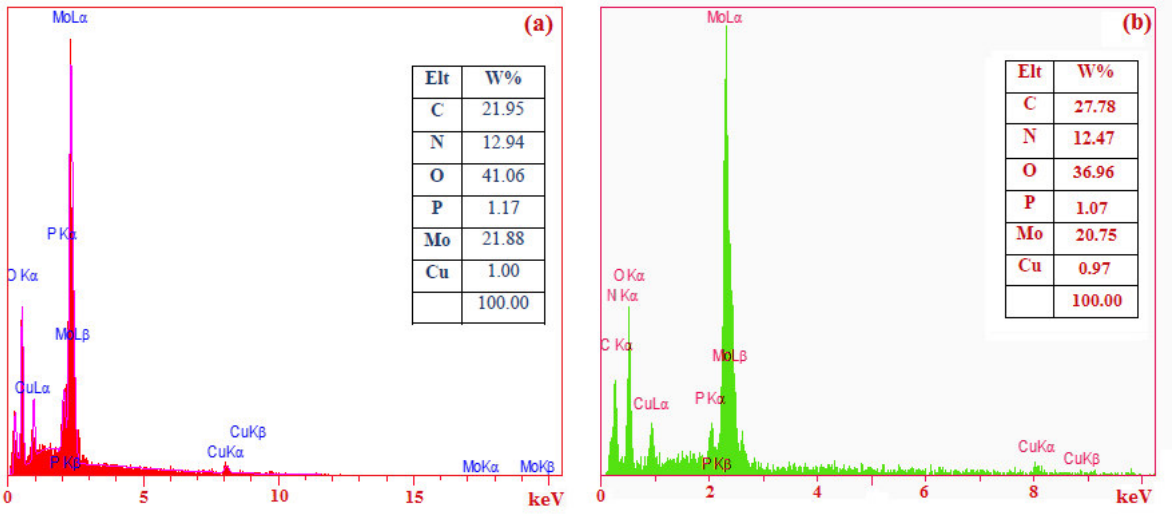

Fig. 6. EDX analysis of (**1**)**:** (a) as nanohybrid powder and (b) as single crystal.

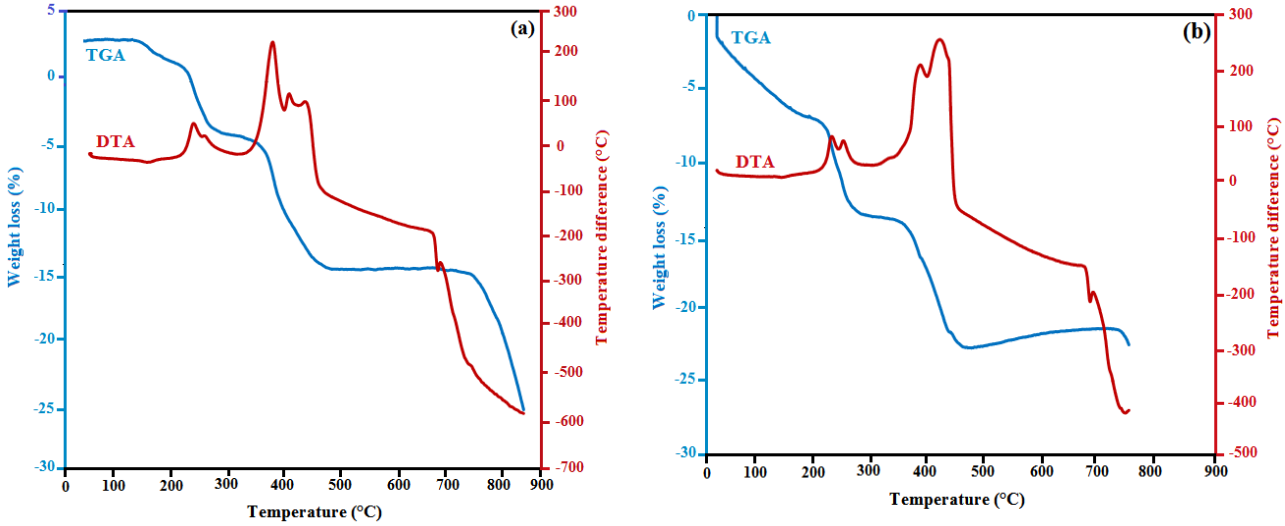

Fig. 7. TG-DTA diagrams of compound (**1**): (a) as single crystal and (b) as nanohybrid.

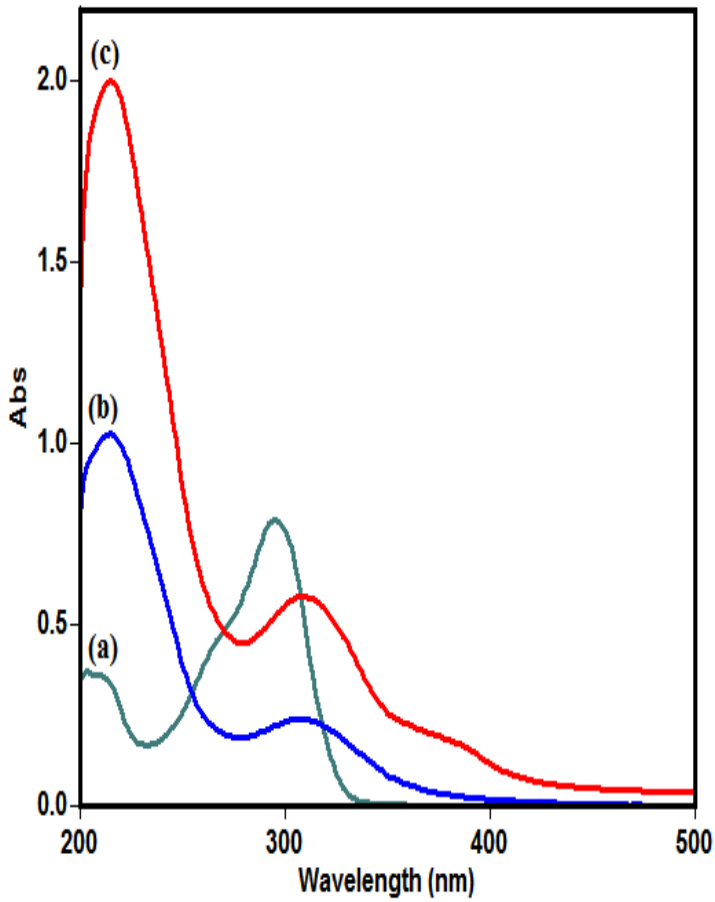

Fig. 8. UV-Vis spectra of the (a) HL, (b) $PMo_{12}O_{40}^{3-}$ polyanion, and (c) nanohybrid (**1**).

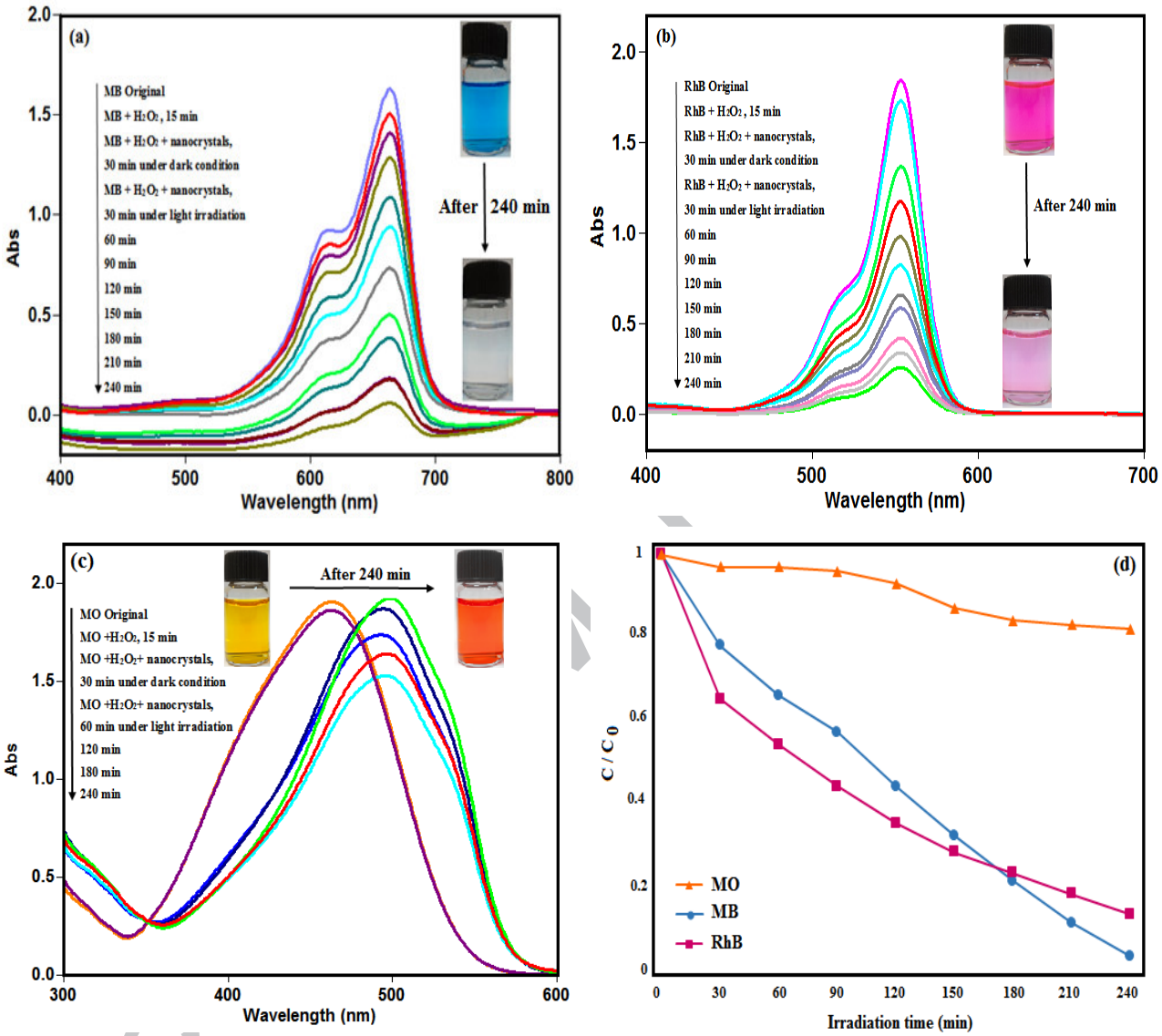

Fig. 9. UV-vis spectral changes of (a) MB, (b) RhB and (c) MO solutions in the presence of (**1**) under irradiation. The inset photos in Fig 8(a)-(c) show the colour change of dyes. (d) Comparison of the concentration changes (C/C_0) of dyes as a function of irradiation time. $[MB]_0$ = 25 mg/L, 50 mL; [photocatalyst (**1**)]$_0$ = 25 mg/50 mL; $[H_2O_2]$ = 0.1 mol/L, 2 mL; Irradiation time = 240 min.

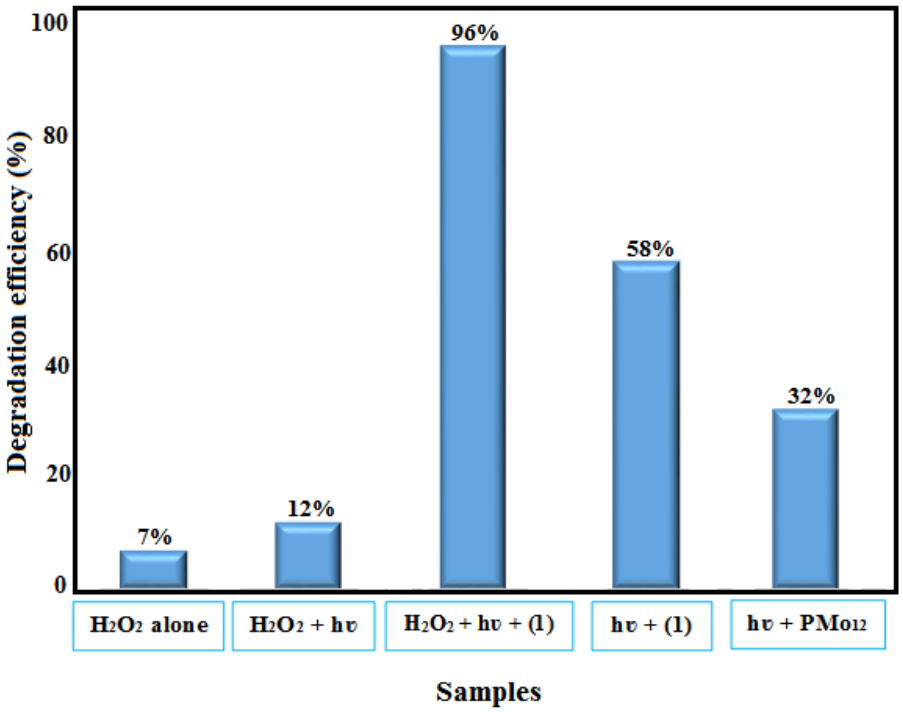

Fig. 10. The photocatalytic degradation percentage of MB under different conditions. $[MB]_0$ = 25 mg/L, 50 mL; [photocatalyst (**1**)]$_0$ = 25 mg/50 mL; $[H_2O_2]$ = 0.1 mol/L, 2 m L; Irradiation time = 240 min.

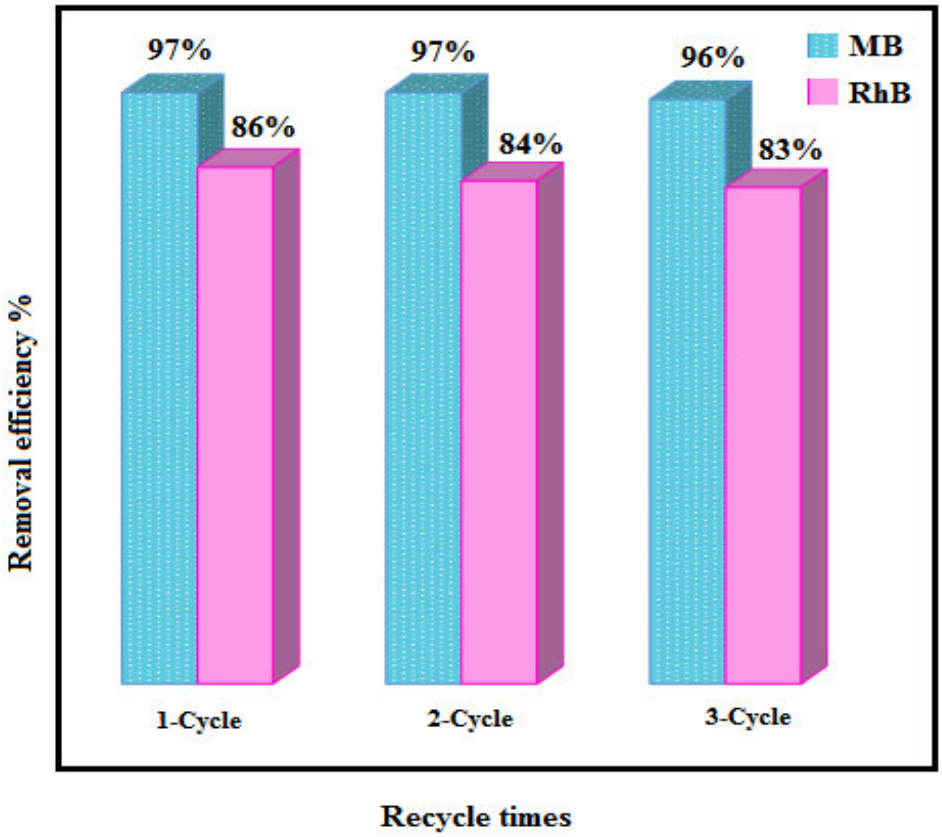

Fig. 11. Photocatalytic degaradation efficiency for MB and RhB with nanohybrid (**1**) as a photocatalyst in different recycling times. $[dye]_0$ = 25 mg/L, 50 mL; [photocatalyst (**1**)]$_0$ = 25 mg/50 mL; $[H_2O_2]$ = 0.1 mol/L, 2 m L; Irradiation time = 240 min.

Graphical abstract-Pictogram

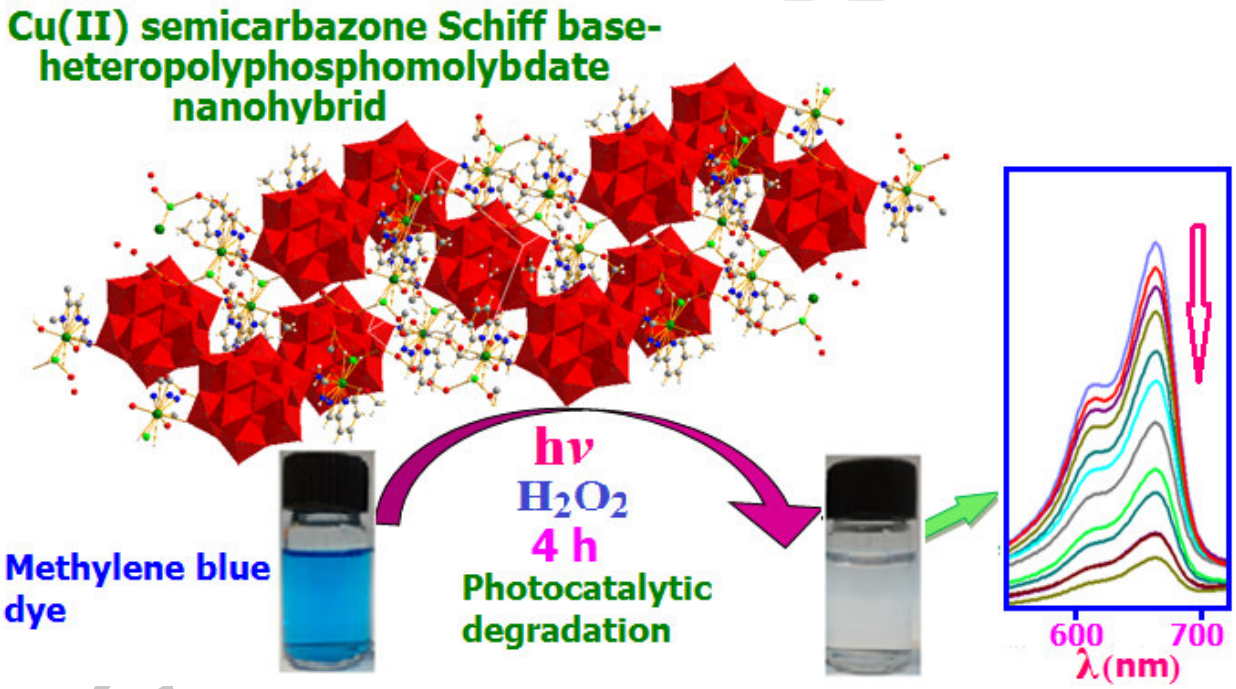

Graphical abstract-synopsis

A new inorganic-organic nanohybrid based on Keggin-type polyoxomolybdate and a copper(II) semicarbazone complex, namely $[Cu_2(HL)_2(PMo_{12}O_{40})(OCH_3)_2(Cl)(H_2O)].8CH_3OH{\cdot}4H_2O$ [HL=pyridine-2-carbaldehyde semicarbazone] (**1**) was synthesized by a sonochemical method and it has been used as an efficient and recoverable photocatalyst for the complete degradation of cationic dyes.